Supporting Information for Publication: The Role of Disorder in NaO_2 and its Implications for Na-O_2 Batteries

Oleg Sapunkov,[†] Vikram Pande,[†] Abhishek Khetan,[‡] and Venkatasubramanian Viswanathan[*,†]

†*Department of Mechanical Engineering, Carnegie Mellon University, Pittsburgh, Pennsylvania 15213*

‡*Institute for Combustion Technology, RWTH, Aachen, Germany, 52056*

E-mail: venkvis@cmu.edu

Computational Parameters

Self-consistent Density Functional Theory (DFT) calculations were performed using the Projector Augmented Wave (PAW) Method as implemented in GPAW.[1] The energy calculations used the Revised PerdewBurkeErnzerhof (RPBE) exchange correlation functional.[2] To correct for electron localization in NaO_2, we incorporated onsite electron repulsion using the Hubbard model, with the Hubbard U applied on the oxygen 2p states in NaO_2. For all investigated structures, the Hubbard U correction was ramped in increments of 0.1 eV.[3–7] All calculations were run with a real-space grid of 0.18 Å spacing, and a 6×6×6 k-point sampling, following the Monkhorst-Pack scheme.[8] Fermi-Dirac smearing of 0.01 eV was used to facilitate convergence and ensure accuracy. The Poisson equation was solved with convergence tolerance of $\epsilon = 10^{-12}$, to ensure electron density is solved precisely, to improve convergence of the calculations. Broyden-type mixing of electron densities was used in the calculation, mixing 5 previous densities with weights of 5%.[9] The spin densities were mixed separately[10] and the calculations were converged to a force of < 0.01 eV/Å.

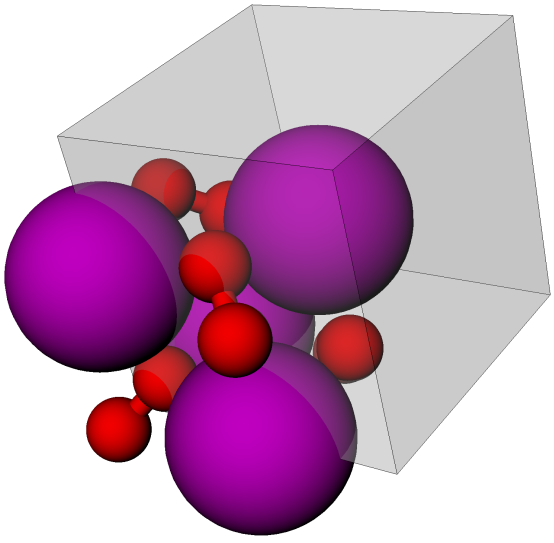

Figure 1: Unit cell of $Fm\bar{3}m$ NaO_2 used in the study.

Density of States

For calculations involving the electronic properties of NaO_2, we used the HSE06 hybrid functional,[11] which has been demonstrated to give accurate bandgap estimates for a broad range of materials.[12] HSE06 is implemented in plane-wave (PW) mode in GPAW, so all structures were re-converged to the same accuracy as in the grid mode mentioned above. PW-mode calculations were first run using PBE, then the HSE06 hybrid functional was applied to correct for the energy levels of various bands. The bandgap was converged with respect to the k-point sampling, PW energy cutoff, and the Fermi-Dirac smearing. After checking convergence, k-point sampling of 8×8×8, PW energy cutoff of 600 eV, and Fermi-Dirac smearing of 0.1 eV were used for fast and accurate convergence. Input structures to the HSE06 bandgap calculations were run using the Hubbard U correction, and bandgap variation was evaluated as a function of U.

Formation Enthalpy Calculations

The enthalpy of formation ΔH_F of a molecule is the enthalpy required to assemble the molecule from individual atoms. ΔH_F is computed as the difference between DFT-calculated internal energy of the assembled molecule and the sum of reference internal energies of constituent species. Thus, the formation enthalpy of NaO_2 was calculated using reference sodium and oxygen energies, given by:

$$\Delta H_{F_{NaO_2}} = E_{NaO_{2DFT}} - E_{Na_{Ref}} - E_{O_{2Ref}} + \Delta pV. \quad (1)$$

The pressure-volume work term, ΔpV, can be disregarded, as it was found to be 5 orders of magnitude lesser than internal energy contributions in formation enthalpy calculations.[13,14] Internal energies for Na, O_2, and NaO_2 were calculated using DFT simulations. Several schemes were used to calculate reference energies for sodium and oxygen, as illustrated in

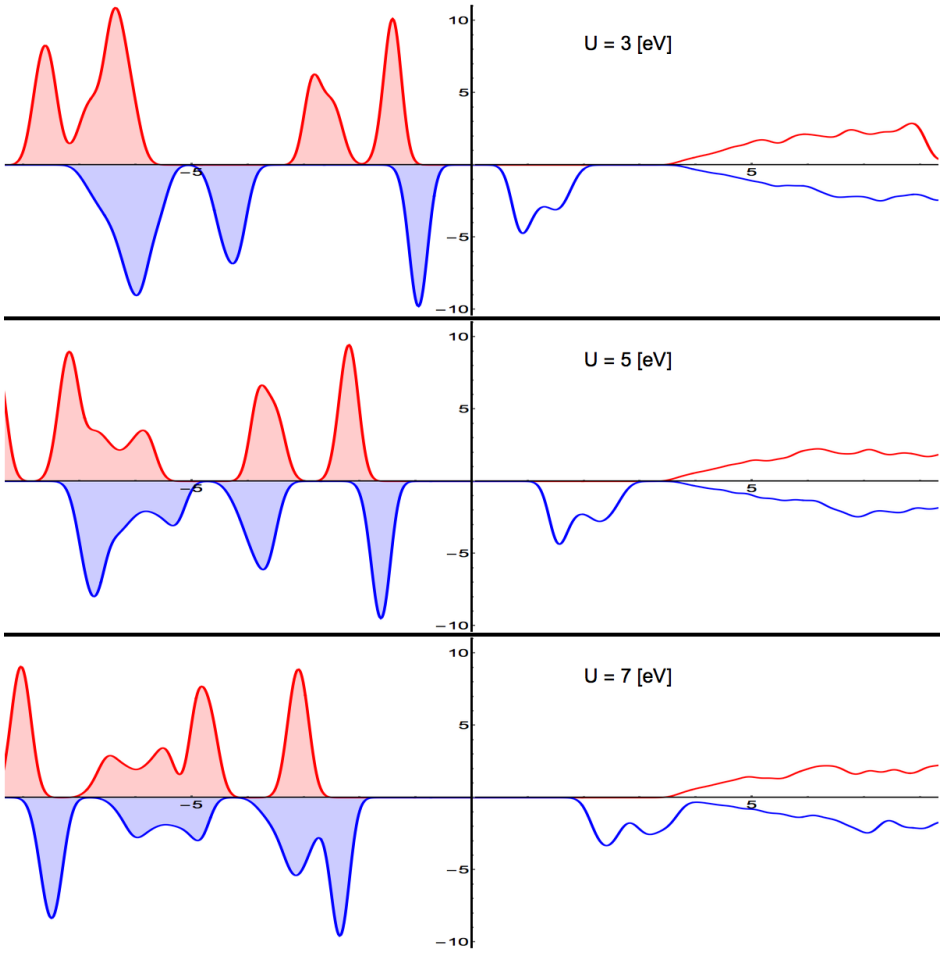

Figure 2: Density of States plots illustrating the widening of the bandgap of NaO_2 using the U correction. These DoS plots have been provided for one of the ferromagnetic phases of NaO_2, but the widening of the bandgap with increasing U is characteristic of all examined phases of NaO_2.

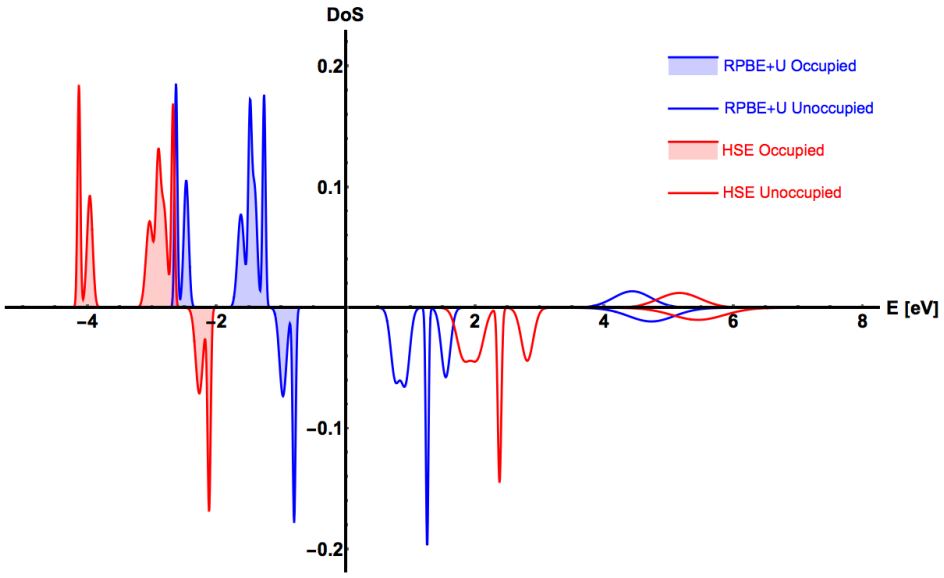

Figure 3: Density of States Plots illustrating the widening of the bandgap of NaO_2 using the HSE correction. Density of States under PBE level of theory is plotted in blue, with filling indicating occupied states. Corresponding Density of States plots under the HSE level of theory are provided in parallel in red, demonstrating the widening of the predicted bandgap using the HSE correction.

Fig. 5.

Initial calculations were run using direct DFT calculations for both the bulk Na reference internal energy and the gaseous O_2 reference internal energy for NaO_2 directly. This scheme is sufficient for the calculation of formation enthalpies of most compounds.

$$E_{Na_{Ref}} = E_{Na_{U_{DFT}}} \tag{2}$$

$$E_{O_{2\,Ref}} = E_{O_{2\,U_{DFT}}} \tag{3}$$

The scheme used the ground state of molecular oxygen: triplet oxygen, which has a non-zero net magnetic moment, since both of its highest-energy electrons, in the 2p π^* orbital, are spin-up electrons, occupying distinct orbitals, following the Pauli Exclusion Principle. The calculation was carried out with spin polarization enabled, with the two oxygen atoms preset to the same net magnetic moment of $+1/2$. In this configuration, the energy of the oxygen was over-stabilized, and the calculated formation enthalpy was too high for all values of the

Hubbard U, as compared to the experimental formation enthalpy.

It is well-known that molecular oxygen is poorly described in DFT, and our first two calculation schemes for the formation enthalpy of NaO_2 were unable to match the experimental formation enthalpy using the DFT-calculated energy of O_2 alone. The energy of oxygen can be more accurately calculated using water as the reference.[15,16] In the first scheme used, reference energy of oxygen was computed using the DFT-calculated internal energies of water and gaseous hydrogen, as well as the experimental formation enthalpy of water. This correction is given by:

$$E_{O_{2\,Ref}} = 2E_{H_2O_{DFT}} - 2E_{H_{2\,DFT}} - \Delta H_{H_2O_{Exp}} \tag{4}$$

DFT-calculated sodium internal energy was used as the sodium reference in this scheme directly, i.e. $E_{Na_{Ref}} = E_{Na_{DFT}}$. The Hubbard U correction was applied on the oxygen atoms in H_2O, to appropriately calculate formation enthalpy of NaO_2 at corresponding values of the Hubbard U. Using this reference energy scheme, we were able to match the formation enthalpy of NaO_2, at a Hubbard U value of approximately 5.5 eV.

We also analyzed a second reference scheme, to correct for the reference energy of bulk Na. It was demonstrated in prior work that formation enthalpies of alkali oxides, peroxides and superoxides are best described when the oxidation state of the metal in the reference compound is matched to the oxidation state of the metal in the compound under investigation.[17,18] Following this scheme, the Na reference energy was calculated using the simulated internal energies of NaCl and gaseous Cl_2, as well as the experimental formation enthalpy of NaCl. The correction is given by:

$$E_{Na_{Ref}} = E_{NaCl_{DFT}} - \frac{1}{2}E_{Cl_{2\,DFT}} - \Delta H_{NaCl_{Exp}} \tag{5}$$

This scheme also made use of the water reference for oxygen energy, as described above. It was found that using both schemes together decreased the Hubbard U required to match the

computed formation enthalpy of NaO_2 to its experimental value, as compared to using the water scheme alone, from approximately 5.5 eV to just over 3 eV, as shown in Fig. 5.

Ising Model

In order to map out the energetic interactions between the magnetic and rotational degrees of freedom, we utilize a modified Ising model. The Ising Model was orginally developed to study properties of interacting lattice systems, such as ferromagnetic materials.[19] In the model, an arbitrary lattice of N sites is set up. A given site i can be filled with a particle with some relevant property specified, such as spin, and is assigned an occupation term, σ_i, where $\sigma_i = 0$ if site i is empty, and $\sigma_i = 1$ if site i is occupied. The energy contribution due to the presence of a particle in site i is designated as the field term, h_i. Energy contributions due to particle interactions in neighboring sites are captured by the nearest-neighbor interaction term, $j_{i,k}$ where i and k are two distinct sites. These nearest-neighbor interactions can be attractive or repulsive. Further interactions can also be accounted for, such as next-nearest-neighbor interactions. These would be assigned a different set of interaction terms $j_{i,k}$. The total energy of the N-site lattice is then calculated as:

$$E = -\sum_{i=1}^{N} h_i \sigma_i - \sum_{\langle ij \rangle} j_{i,k} \sigma_i \sigma_k \tag{6}$$

The Ising Model allows derivation of a reduced-order Hamiltonian for the system under consideration. Simulated formation enthapies are used to calculate relevant Ising Model coefficients for the system. Through the use of coefficients derived with the Ising Model, the new Hamiltonian can be implemented in a Monte Carlo simulation of larger bulk structures. These simulations introduce and allow the quantification of the effect of thermal disorder on the system.

Metropolis Monte Carlo

Coefficients derived from the Ising Model were then used to simulate larger bulk cells with higher degree of disorder, to predict their formation enthalpies. In this model, we accounted for periodic boundary conditions in all directions to make our structure characteristic of a bulk material.

Systems were studied using the Markov Chain Monte Carlo Method,[20,21] modified with the Metropolis-Hastings Algorithm.[22] Since our simulated NaO_2 structures only included nearest-neighbor interactions, and no longer-range interactions, our Ising Model analysis likewise was limited only to nearest-neighbor interactions. We accounted for both two-body and three-body nearest-neighbor interactions. Derived nearest-neighbor $j_{2:i,k}$ and $j_{3:i,k,l}$ were used to calculate the full system formation enthalpy through the Ising model for these larger, bulk-like systems.

At the beginning of the Monte Carlo simulation, a fully-organized initial supercell structure was set up. Each individual trial step taken in the Monte Carlo simulation consisted of switching a randomly selected O_2 dimer in the bulk NaO_2 structure to one of the other available configurations for that dimer. Before and after the switch, full system formation enthalpy was calculated using the 2- and 3-body Ising Model coefficients derived earlier. To make the calculation efficient, only nearest-neighbor interactions around the altered dimer itself were calculated, since the remainder of the system maintained the same net enthalpy before and after the trial step executed. The Metropolis Algorithm was used to decide whether to accept the trial step or not:

1. A uniformly distributed random real number ϵ was chosen, between 0 and 1
2. A coefficient, called here β, was calculated: $\beta = e^{(-1/k_B T)*(E_{trial}-E_{ref})}$
3. The two numbers were compared
4. If $\epsilon \leq \beta$, the trial step was accepted, the new structure was saved as the reference

structure for the next step.

5. If instead $\epsilon > \beta$, the trial step was rejected and the system was reverted back to the earlier, reference structure.

At the end of every trial step, the system formation enthalpy and entropy were recorded for further analysis.

To explore high-temperature, high-energy phases of bulk NaO_2, each simulation was initialized with a fully-organized supercell structure, composed of N x N x N cells of configuration AAAA-PPPP. Initial system temperature used in the Metropolis-Hastings scheme was raised to 1252 K, to examine if the simulated bulk material would maintain long-range orientational or magnetic order at high temperature. The structure was simulated at 1252 Kelvin for a number of steps N_{st} sufficient to reach and maintain stable system energy. The required N_{st} was scaled with the supercell size N, as $N_{st} = 15000 * (\mathrm{N}/3)^2$. Once the energy of the structure was stabilized at the initial high temperature, the system was annealed[23] in temperature steps of 0.25 K, down to 2 K. At each 50 K increment, the structure was held for an equivalent N_{st}, and both formation enthalpy and configurational entropy data was collected for analysis. This scheme worked robustly for the system studied, which contained between 256 and 1372 sites. Both entropy and formation enthalpy, per oxygen dimer contained, remained consistent for all supercell sizes investigated.

The simulation was used to output data regarding the formation enthalpy of the bulk supercell, per formula unit, and the energy contribution by the configurational entropy of the bulk supercell ($\mathrm{T} * \mathrm{S}$), per formula unit, as recorded at the end of every trial step. Configurational entropy was calculated as the logarithm of the number of configurations with the same proportions of oxygen dimers of different types. If there are M distinct dimer types available, the total number of possible configurations, Ω, of the full structure can be

calculated using the complete multinomial coefficient:

$$\Omega = \prod_{j=1}^{M} \binom{\sum_{i=j}^{M} N_i}{N_j} \tag{7}$$

where i, j refer to the available configurations of dimers and N_i, N_j refer to the number of dimers of a particular configuration present in the supercell. The configurational entropy is then simply calculated by Boltzmann's Entropy Formula: $S_{Conf} = k_B \log \Omega$.

Tables of Calculated Values

Table 1: Calculated formation enthalpies of NaO_2 bulk structures, in eV. AAAA-PPPN and ABCD-PPPN structures could not be converged at a Hubbard U value of 2 eV since it did not localize the highest-energy electrons on the oxygen dimers sufficiently to stabilize the structure.

Hubbard U	2	3	4	5	6	7
AAAA-PPNN	-2.523	-2.675	-2.846	-3.036	-3.248	-3.480
AAAA-PPPN		-2.533	-2.662	-2.806	-2.968	-3.146
AAAA-PPPP	-2.428	-2.538	-2.668	-2.810	-2.971	-3.145
AAAB-PPNN	-2.653	-2.736	-2.977	-3.169	-3.382	-3.598
AAAB-PPNP	-2.658	-2.810	-2.900	-3.168	-3.362	-3.609
AAAB-PPPN	-2.658	-2.810	-2.980	-3.164	-3.382	-3.611
AAAB-PPPP	-2.638	-2.804	-2.969	-3.171	-3.383	-3.616
AABB-PNPN	-2.603	-2.744	-2.906	-3.088	-3.290	-3.521
AABB-PPNN	-2.600	-2.740	-2.996	-3.192	-3.409	-3.646
AABB-PPPN	-2.600	-2.742	-2.906	-3.089	-3.293	-3.536
AABB-PPPP	-2.598	-2.740	-2.996	-3.192	-3.409	-3.517
AABC-PNPN	-2.655	-2.802	-2.974	-3.160	-3.375	-3.607
AABC-PNPP	-2.654	-2.804	-2.973	-3.162	-3.366	-3.662
AABC-PPNN	-2.655	-2.803	-2.973	-3.161	-3.372	-3.666
AABC-PPPN	-2.651	-2.802	-2.973	-3.156	-3.431	-3.614
AABC-PPPP	-2.652	-2.804	-2.974	-3.162	-3.433	-3.665
ABCD-PPNN	-2.478	-2.621	-2.785	-3.017	-3.171	-3.396
ABCD-PPPN		-2.484	-2.608	-2.806	-2.968	-3.146
ABCD-PPPP	-2.371	-2.494	-2.606	-2.755	-2.910	-3.148

Table 2: Table of bandgaps calculated with the hybrid functional HSE06. Antiferromagnetic structures show equivalently high bandgap in both spin channels, while ferromagnetic structures show a higher bandgap in the positive spin channel and a lower bandgap in the negative spin channel. Ferromagnetic structures of intermediate geometric disorder have a smaller disparity in spins than structures fully-ordered or fully-disordered.

Hubbard U	U3		U4		U5		U6		U7	
Spin	s↑	s↓	s↑	s↓	s↑	s↓	s↑	s↓	s↑	s↓
AAAA-PPPP	6.65	1.26	7.3	1.85	7.57	1.74	8.1	1.97	8.71	2.18
AAAB-PPPP	7.43	3.69	7.85	4.09	8.35	5.14	8.89	5.93	9.49	6.76
AABB-PPPP	7.03	3.96	7.37	4.64	7.78	5.33	8.24	6.07	8.76	6.68
AABC-PPPP	7.3	3.92	7.72	4.65	8.15	5.35	*	*	9.84	6.82
ABCD-PPPP	5.91	1.32	6.49	1.92	6.88	1.62	8.11	1.97	8.7	2.17
AAAA-PPNN	3.82	3.82	4.54	4.54	5.27	5.27	6.07	6.07	6.91	6.91
AAAB-PPNN	3.91	3.91	4.59	4.59	5.32	5.32	6.1	6.1	6.92	6.92
AABB-PPNN	4.13	4.13	4.83	4.83	5.57	5.57	6.35	6.35	7.21	7.21
AABB-PNPN	4.21	4.21	4.89	4.89	5.59	5.59	6.36	6.36	6.89	6.89
AABC-PPNN	4.39	4.13	5.1	5.1	5.84	5.55	*	*	*	*
ABCD-PPNN	3.94	3.94	4.66	4.66	5.42	5.42	6.23	6.23	7.12	7.12
AABC-PNPN	*	*	*	*	*	*	*	*	*	*

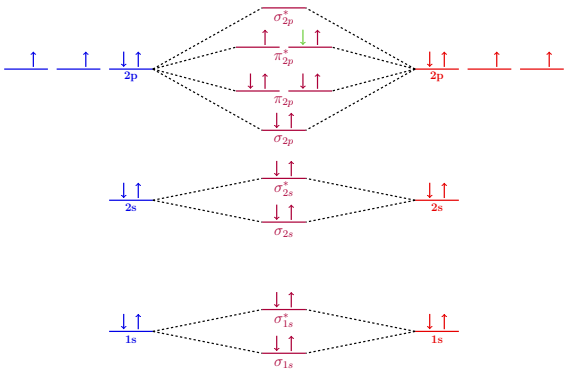

Figure 4: Molecular Orbital Diagram of O_2^-. The external electron added to the O_2 molecule falls into the $\pi^*_(2p)$ orbital, already occupied by two spin-up electrons. This leaves oxygen with only one unpaired electron, which makes it weakly paramagnetic.

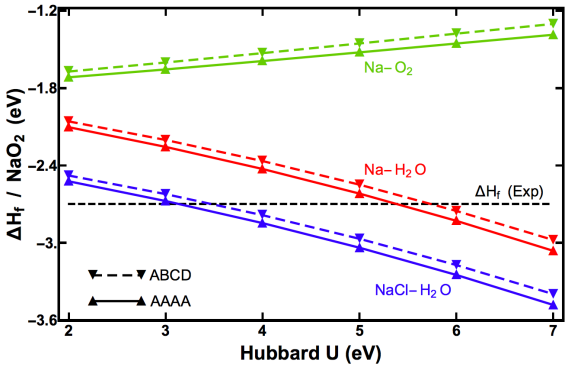

Figure 5: Performance of different schemes used for Formation Enthalpy calculations. The simulations done with oxygen energy calculations to provide the O_2 reference energy gave the poorest results, since oxygen is poorly handled in DFT simulations. Correcting the oxygen energy with the water scheme improved the energy calculations tremendously, and allowed to match experimental formation enthalpy at a Hubbard U value around 6 eV. The required value of the Hubbard U was decreased to 3 eV by applying the scheme which accounted for the correct sodium ion oxidation state, using NaCl as the reference calculation.

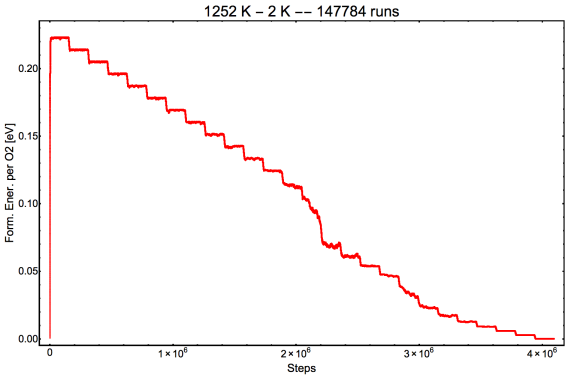

Figure 6: Example of the annealing scheme used with the Metropolis Monte Carlo simulations. The system was initialized at high temperature, and then annealed down to just over absolute zero, in steps of 0.25 K. Every 50 K, the system was held at a constant temperature long enough to reach stability and take data for further analysis. Data taken at this 50 K intervals was used to produce the temperature-dependent plots of formation enthalpy and the entropic energy contribution

References

(1) Enkovaara, J.; Rostgaard, C.; Mortensen, J. J.; Chen, J.; Dułak, M.; Ferrighi, L.; Gavnholt, J.; Glinsvad, C.; Haikola, V.; Hansen, H. et al. Electronic structure calculations with GPAW: a real-space implementation of the projector augmented-wave method. *J. Phys. Condens. Matter* **2010**, *22*, 253202.

(2) Hammer, B.; Hansen, L. B.; Nørskov, J. K. Improved adsorption energetics within density-functional theory using revised Perdew-Burke-Ernzerhof functionals. *Phys. Rev. B* **1999**, *59*, 7413.

(3) Hubbard, J. Electron correlations in narrow energy bands. Proceedings of the royal society of london a: mathematical, physical and engineering sciences. 1963; pp 238–257.

(4) Anisimov, V. I.; Zaanen, J.; Andersen, O. K. Band theory and Mott insulators: Hubbard U instead of Stoner I. *Phys. Rev. B* **1991**, *44*, 943.

(5) Himmetoglu, B.; Floris, A.; Gironcoli, S.; Cococcioni, M. Hubbard-corrected DFT energy functionals: The LDA+ U description of correlated systems. *Int. J. Quantum Chem.* **2014**, *114*, 14–49.

(6) García-Mota, M.; Bajdich, M.; Viswanathan, V.; Vojvodic, A.; Bell, A. T.; Nørskov, J. K. Importance of correlation in determining electrocatalytic oxygen evolution activity on cobalt oxides. *J. Phys. Chem. C* **2012**, *116*, 21077–21082.

(7) Meredig, B.; Thompson, A.; Hansen, H.; Wolverton, C.; Van de Walle, A. Method for locating low-energy solutions within DFT+ U. *Phys. Rev. B* **2010**, *82*, 195128.

(8) Monkhorst, H. J.; Pack, J. D. Special points for Brillouin-zone integrations. *Phys. Rev. B* **1976**, *13*, 5188.

(9) Johnson, D. D. Modified Broyden's method for accelerating convergence in self-consistent calculations. *Phys. Rev. B* **1988**, *38*, 12807.

(10) Srivastava, G. Broyden's method for self-consistent field convergence acceleration. *J. Phys. A: Math. Gen.* **1984**, *17*, L317.

(11) Heyd, J.; Scuseria, G. E.; Ernzerhof, M. Hybrid functionals based on a screened Coulomb potential. *J. Chem. Phys.* **2003**, *118*, 8207–8215.

(12) Deák, P.; Aradi, B.; Frauenheim, T.; Janzén, E.; Gali, A. Accurate defect levels obtained from the HSE06 range-separated hybrid functional. *Phys. Rev. B* **2010**, *81*, 153203.

(13) Aydinol, M.; Kohan, A.; Ceder, G.; Cho, K.; Joannopoulos, J. Ab initio study of lithium intercalation in metal oxides and metal dichalcogenides. *Phys. Rev. B* **1997**, *56*, 1354.

(14) Obrovac, M.; Chevrier, V. Alloy negative electrodes for Li-ion batteries. *Chem. Rev.* **2014**, *114*, 11444–11502.

(15) Rossmeisl, J.; Logadottir, A.; Nørskov, J. K. Electrolysis of water on (oxidized) metal surfaces. *Chem. Phys.* **2005**, *319*, 178–184.

(16) Droghetti, A.; Pemmaraju, C.; Sanvito, S. Predicting d 0 magnetism: Self-interaction correction scheme. *Phys. Rev. B* **2008**, *78*, 140404.

(17) Wang, L.; Maxisch, T.; Ceder, G. Oxidation energies of transition metal oxides within the GGA+ U framework. *Phys. Rev. B* **2006**, *73*, 195107.

(18) Christensen, R.; Hummelshøj, J. S.; Hansen, H. A.; Vegge, T. Reducing Systematic Errors in Oxide Species with Density Functional Theory Calculations. *J. Phys. Chem. C* **2015**, *119*, 17596–17601.

(19) Ising, E. Beitrag zur theorie des ferromagnetismus. *Z. Phys. A* **1925**, *31*, 253–258.

(20) Gilks, W. R. *Markov chain monte carlo*; Wiley Online Library, 2005.

(21) Hastings, W. K. Monte Carlo sampling methods using Markov chains and their applications. *Biometrika* **1970**, *57*, 97–109.

(22) Chib, S.; Greenberg, E. Understanding the metropolis-hastings algorithm. *The American Statistician* **1995**, *49*, 327–335.

(23) Vanderbilt, D.; Louie, S. G. A Monte Carlo simulated annealing approach to optimization over continuous variables. *J. Comput. Phys.* **1984**, *56*, 259–271.